

# Low metallicity AGB models: H profile in the $^{13}\text{C}$ -pocket and the effect on the $s$ -process

S. Bisterzo<sup>1</sup> and S. Cristallo<sup>2,3</sup>

<sup>1</sup> Dipartimento di Fisica Generale, Università di Torino, 10125 (To) Italy

<sup>2</sup> Departamento de Física Teórica y del Cosmos, Universidad de Granada, Campus de Fuentenueva, 18071 Granada, Spain

<sup>3</sup> INAF Osservatorio Astronomico di Collurania, via M. Maggini, 64100 Teramo, Italy  
e-mail: bisterzo@ph.unito.it

**Abstract.** The  $^{13}\text{C}(\alpha, n)^{16}\text{O}$  reaction is the major neutron source in low mass asymptotic giant branch (AGB) stars, where the main and the strong  $s$  process components are synthesised. After a third dredge-up (TDU) episode,  $^{13}\text{C}$  burns radiatively in a thin pocket which forms in the top layers of the He-intershell, by proton capture on the abundant  $^{12}\text{C}$ . Therefore, a mixing of a few protons from the H-rich envelope into the He-rich region is requested. However, the origin and the efficiency of this mixing episode are still matter of debate and, consequently, the formation of the  $^{13}\text{C}$ -pocket represents a significative source of uncertainty affecting AGB models. We analyse the effects on the nucleosynthesis of the  $s$ -elements caused by the variation of the hydrogen profile in the region where the  $^{13}\text{C}$ -pocket forms for an AGB model with  $M = 2 M_{\odot}$  and  $[\text{Fe}/\text{H}] = -2.3$ . In particular, we concentrate on three isotopes ( $^{89}\text{Y}$ ,  $^{139}\text{La}$  and  $^{208}\text{Pb}$ ), chosen as representative of the three  $s$ -process peaks.

**Key words.** Stars: C ans s rich – Stars: abundances – Stars: nucleosynthesis

## 1. Introduction

During their thermally pulsing (TP) phase, low mass asymptotic giant branch (AGB) stars are the site of the main and the strong component of the  $s$ -process, which is the major responsible for the nucleosynthesis of half the nuclei from Sr to Pb-Bi. After a limited number of pulses, the convective envelope penetrates into the He-intershell at the quenching of each convective instability, mixing freshly synthesized  $^4\text{He}$ ,  $^{12}\text{C}$ , and  $s$ -process elements to the surface (third dredge-up, TDU).

The major neutron source in low mass AGB

stars is the  $^{13}\text{C}(\alpha, n)^{16}\text{O}$  reaction, which burns radiatively during the interpulse period in a thin region at the top of the He-intershell ( $^{13}\text{C}$ -pocket). The physical mechanism that allows the formation of the  $^{13}\text{C}$ -pocket is a debated problem. A small amount of protons is assumed to penetrate from the envelope into the He-intershell during TDU episodes (Iben & Renzini 1982). Then, at H reignition, a large amount of  $^{13}\text{C}$  is synthesised in the top layers of the intershell via the  $^{12}\text{C}(\text{p}, \gamma)^{13}\text{N}(\beta^+ \nu)^{13}\text{C}$  nuclear chain. This  $^{13}\text{C}$  is of primary origin and, therefore, independent of the metallicity. During the interpulse, the H-burning shell advances in mass, compressing and heating the underlying material, and at  $T \sim 0.9 \times 10^8$  K

---

Send offprint requests to: P. Bonifacio

the  $^{13}\text{C}(\alpha, n)^{16}\text{O}$  reaction starts releasing neutrons in radiative conditions. Later on, the synthesised  $s$ -process nuclei are engulfed and diluted in the next convective region generated by TP.

Different evolutionary and post-process codes have been developed in the last years to understand the nucleosynthesis in low mass AGB stars (e.g., Straniero et al. 1995, 2003; Gallino et al. 1998; Goriely & Mowlavi 2000; Karakas & Lattanzio 2003, 2007; Campbell & Lattanzio 2008; Straniero, Gallino & Cristallo 2006). Several mechanisms have been proposed to reproduce the mixing leading to the  $^{13}\text{C}$ -pocket formation: semi-convection (Hollowell & Iben 1988), models including rotation (Langer et al. 1999; Herwig et al. 2003; Siess et al. 2004), gravity waves (Denissenkov & Tout 2003), exponential diffusive overshoot at the borders of all convective zones (Herwig et al. 1997), opacity-induced overshoot at the base of the convective envelope (Straniero et al. 2006). A clear answer to the properties of such mixing has not been reached yet.

We test here the effects on the nucleosynthesis of the  $s$  elements by adopting different H profiles in the region of the  $^{13}\text{C}$ -pocket forming after the 1<sup>st</sup> TDU of an AGB model with initial  $M = 2 M_{\odot}$  and  $[\text{Fe}/\text{H}] = -2.3$ . Comparison between full evolutionary FRANEC (Frascati Raphson-Newton Evolutionary Code) models (Cristallo et al. 2009, hereafter C09) and FRANEC models coupled with a post-process nucleosynthesis method (Gallino et al. 1998; Bisterzo et al. 2010) are presented.

## 2. Results

C09 introduce a mixing algorithm depending on a free parameter<sup>1</sup> in their full evolutionary models to mimics the formation of a transition zone between the fully convective envelope and the radiatively stable H-exhausted core. Thus, a partial mixing of protons takes place leading to the formation of a  $^{13}\text{C}$  rich layer. Its mass and profile decrease with the number of pulses (see C09, their Fig.s 4 and 8).

<sup>1</sup> See C09 for the procedure followed to calibrate it.

Fig. 1, top panel, shows this region. In the uppermost layers of the pocket, where protons are more abundant, the  $^{13}\text{C}$ -pocket is overlapped with a  $^{14}\text{N}$ -pocket, which forms via the  $^{13}\text{C}(\text{p}, \gamma)^{14}\text{N}$  reaction.  $^{14}\text{N}$  acts as a neutron poison via the resonant reaction  $^{14}\text{N}(\text{n}, \text{p})^{14}\text{C}$ , thus subtracting neutrons to the nucleosynthesis of the  $s$ -process elements. Fig. 1, bottom panel, shows the same mass region at the end of the  $^{13}\text{C}$  burning. We concentrate on three isotopes,  $^{89}\text{Y}$ ,  $^{139}\text{La}$  and  $^{208}\text{Pb}$ , chosen as representative of the three  $s$ -process peaks. As expected, at this low metallicity (Gallino et al. 1998), a large amount of  $^{208}\text{Pb}$  is produced. Maximum Pb production occurs in the central layers of the pocket, where  $X(^{13}\text{C}) > X(^{14}\text{N})$  (we find  $X(^{208}\text{Pb}) = 4.5 \times 10^{-5}$ ), while Y and La show definitely lower abundances:  $X(^{89}\text{Y}) \sim X(^{139}\text{La}) \sim 6 \times 10^{-9}$ . In the outer and inner regions of the pocket, however,  $^{89}\text{Y}$  and  $^{139}\text{La}$  show peaked distributions. Note that, in the outer tail,  $s$ -process elements are efficiently synthesised even if  $X(^{13}\text{C}) < X(^{14}\text{N})$ .

In order to test the effect of these tails on Y, La and Pb with different H profiles, we use the post-process nucleosynthesis models described by Bisterzo et al. (2010). We adopt the H profile of Gallino et al. (1998; case ST; their Fig. 2). Then, we introduce a further region in the pocket (with mass  $M = 4 \times 10^{-4} M_{\odot}$ ) where we change the abundances of  $^{13}\text{C}$  and  $^{14}\text{N}$  to simulate different H profiles in the tails. Therefore, we multiply or divide by different factors the  $^{13}\text{C}$  and  $^{14}\text{N}$  abundances in the pocket<sup>2</sup>. Note that the H profile and the mass of the pocket are kept constant pulse by pulse. The envelope abundances of the two  $s$ -process indexes  $[\text{La}/\text{Y}]$  and  $[\text{Pb}/\text{La}]$  obtained with the post-process method are show in Tables 1 and 2. In Table 1, first group, we show the results computed with standard  $^{13}\text{C}$ -pockets (i.e. with 3 zones as in Gallino et al. 1998) for various  $^{13}\text{C}$ -pocket efficiencies (from  $\text{ST} \times 2$  down to  $\text{ST}/24$ ). These results are compared with models with an added zone 4 with  $X(^{13}\text{C}) < X(^{14}\text{N})$  (Table 1, second group). This has been done

<sup>2</sup> In fact, a range of  $^{13}\text{C}$ -pockets is introduced in order to interpret the spread in the  $s$ -elements observed in CEMP- $s$  stars.

to simulate the effect induced by the outer tail of the pocket shown in Fig. 1 by C09 model on post-process calculations results. C09 obtain a final  $[\text{La}/\text{Y}] = 0.45$  and  $[\text{Pb}/\text{La}] = 1.30$ . With the post-process method and a range of standard  $^{13}\text{C}$ -pockets,  $[\text{La}/\text{Y}]$  reaches a maximum value of  $\sim 0.9$  (case ST/6) and  $[\text{Pb}/\text{La}] \sim 2.2$  (case ST/1.5). When adding the zone 4, minimal variations are found for large and low  $^{13}\text{C}$ -pocket efficiencies, while appreciable differences are found in the intermediate cases. For large  $^{13}\text{C}$  abundances (case ST  $\times 2$ ), the addition of zone 4 leads to a large production of light elements (Ne, Na, Mg), whose poisoning effect induces a slightly decrease of the final  $s$ -process element surface overabundances. For very low  $^{13}\text{C}$  efficiencies the  $s$ -process production is mainly due to the  $^{22}\text{Ne}(\alpha, n)^{25}\text{Mg}$  reaction (Bisterzo et al. 2010), minimizing the effects of additional  $^{13}\text{C}$  and  $^{14}\text{N}$ . For intermediate cases, instead, the introduction of the zone 4 reduces the maximum  $[\text{La}/\text{Y}]$  to  $\sim 0.5$  dex and the maximum  $[\text{Pb}/\text{La}]$  to  $\sim 1.6$  dex. In Table 2 we select the highest  $^{13}\text{C}$ -pocket case (case ST  $\times 2$ ) and we test the effect of an added zone 4 with different  $X(^{13}\text{C})$  values ( $X(^{14}\text{N})$  is assumed to be negligible). We choose the ST  $\times 2$  case because previous comparisons done at larger metallicities (C09) indicate that the best agreement between post-process and full evolutionary models is found with this case. The standard case with 3 zones only (II column) gives  $[\text{La}/\text{Y}] = 0.50$  and  $[\text{Pb}/\text{La}] = 2.04$ , while the addition of a zone 4 with  $X(^{13}\text{C}) = 3.8\text{E-}4$  (test III) definitely lowers the  $[\text{Pb}/\text{La}]$  ratio (1.47) leaving practically untouched the  $[\text{La}/\text{Y}]$  ratio (0.56). Thus, a reasonable agreement between this test and C09 is found even at such low metallicities. Verified that the tails of the  $^{13}\text{C}$ -pocket affect the  $s$  distribution, one may constrain the choice of the H profile through a study of spectroscopic observations in CEMP- $s$  stars. Note that, for disk metallicities, the tails of the pocket do not influence sensibly the  $s$  distribution.

### 3. Conclusions

The maximum amount of  $^{13}\text{C}$  and  $^{14}\text{N}$  in the pocket and different hydrogen profiles (and

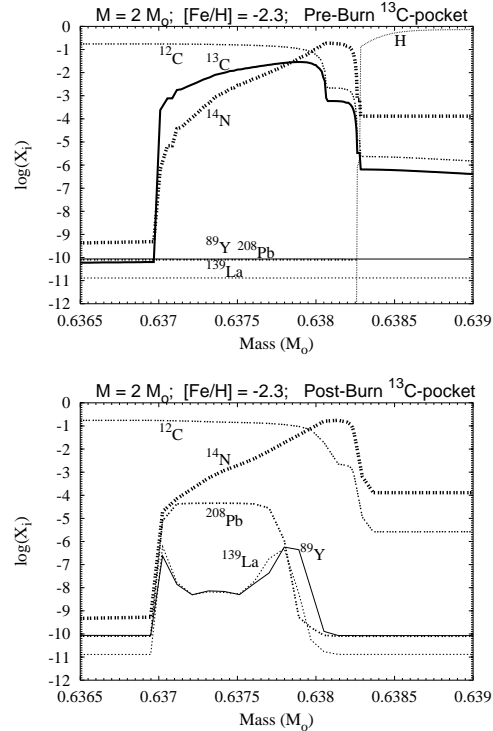


**Fig. 1.**  $^{13}\text{C}$ -pocket mass region for a full evolutionary AGB model of  $M = 2 M_{\odot}$  and  $[\text{Fe}/\text{H}] = -2.3$  (C09) after the first TDU, at the pocket formation (top panel) and at the end of the  $^{13}\text{C}$  burning (bottom panel).

therefore the amount of  $^{13}\text{C}$  and  $^{14}\text{N}$  in the tails of the pocket) modify the  $s$  abundance distribution. In particular, the  $s$ -process indexes  $[\text{La}/\text{Y}]$  and  $[\text{Pb}/\text{La}]$  are sensitive to the tails of the pocket. At  $[\text{Fe}/\text{H}] = -2.3$ , a large amount of  $^{208}\text{Pb}$  is produced when  $X(^{13}\text{C}) > X(^{14}\text{N})$ . A first interesting consequence caused by the addition of an outer tail in the pocket with  $X(^{13}\text{C}) < X(^{14}\text{N})$  is that the maximum  $[\text{La}/\text{Y}]$  value attained with different  $^{13}\text{C}$ -efficiencies is reduced to  $\sim 0.5$ . Moreover, when assuming a calibrated extra  $X(^{13}\text{C})$  in the tails of the pocket, the maximum  $[\text{Pb}/\text{La}]$  is reduced to 1.4 dex. Comparison between theory and observations in CEMP- $s$  stars are then needed in order to constrain the choice of the H profile in the central and outer regions of the  $^{13}\text{C}$ -pocket during AGB nucleosynthesis.

**Table 1.** Envelope abundances of [Y/Fe], [La/Fe], [Pb/Fe] and their ratios [La/Y] and [Pb/La] for a post-process model of  $M = 2 M_{\odot}$  and  $[\text{Fe}/\text{H}] = -2.3$  and various  $^{13}\text{C}$ -pocket efficiencies (from  $\text{ST} \times 2$  down to  $\text{ST}/24$ ). The first group lists the results obtained with the standard  $^{13}\text{C}$ -pocket, while in the second group a further zone 4 with  $X(^{13}\text{C}) < X(^{14}\text{N})$  is added.

| Cases                                 | ST $\times$ 2 | ST     | ST/1.5 | ST/2   | ST/6   | ST/12  | ST/24  |
|---------------------------------------|---------------|--------|--------|--------|--------|--------|--------|
| [Y/Fe]                                | 1.68          | 1.39   | 1.33   | 1.35   | 1.98   | 2.35   | 2.45   |
| [La/Fe]                               | 2.18          | 1.88   | 1.92   | 2.10   | 2.85   | 2.94   | 2.71   |
| [Pb/Fe]                               | 4.22          | 4.12   | 4.09   | 4.06   | 3.82   | 3.44   | 2.69   |
| [La/Y]                                | 0.50          | 0.49   | 0.59   | 0.75   | 0.87   | 0.59   | 0.26   |
| [Pb/La]                               | 2.04          | 2.24   | 2.17   | 1.96   | 0.97   | 0.50   | -0.02  |
| $X(^{13}\text{C})=$                   | 7.2E-2        | 3.7E-2 | 2.5E-2 | 1.9E-2 | 6.2E-3 | 3.1E-3 | 1.6E-3 |
| $X(^{14}\text{N})=$                   | 2.7E-1        | 1.4E-1 | 9.3E-2 | 7.1E-2 | 2.3E-2 | 1.2E-2 | 5.8E-3 |
| zone 4                                |               |        |        |        |        |        |        |
| $X(^{13}\text{C}) < X(^{14}\text{N})$ |               |        |        |        |        |        |        |
| [Y/Fe]                                | 1.58          | 1.75   | 1.89   | 2.00   | 2.40   | 2.58   | 2.64   |
| [La/Fe]                               | 2.10          | 2.25   | 2.42   | 2.54   | 2.92   | 2.97   | 2.80   |
| [Pb/Fe]                               | 4.04          | 4.02   | 3.99   | 3.97   | 3.76   | 3.43   | 2.84   |
| [La/Y]                                | 0.52          | 0.50   | 0.53   | 0.54   | 0.52   | 0.39   | 0.16   |
| [Pb/La]                               | 1.94          | 1.77   | 1.57   | 1.43   | 0.84   | 0.46   | 0.04   |

**Table 2.** The same as Table 1, but for a case  $\text{ST} \times 2$  and an added zone 4 with different  $X(^{13}\text{C})$  values, from 0 (standard case) up to 4.3E-3.  $X(^{14}\text{N})$  is assumed to be negligible. In the last column the results obtained by C09 are listed.

| zone 4,<br>$X(^{13}\text{C})$ | standard<br>0.0 | I test<br>2.9E-4 | II test<br>3.5E-4 | III test<br>3.8E-4 | IV test<br>4.8E-4 | V test<br>5.8E-4 | VI test<br>1.2E-3 | VII test<br>4.3E-3 | C09  |
|-------------------------------|-----------------|------------------|-------------------|--------------------|-------------------|------------------|-------------------|--------------------|------|
| [Y/Fe]                        | 1.68            | 2.23             | 2.21              | 2.19               | 2.09              | 1.97             | 1.74              | 1.75               | 1.12 |
| [La/Fe]                       | 2.18            | 2.60             | 2.65              | 2.75               | 2.80              | 2.76             | 2.48              | 2.27               | 1.57 |
| [Pb/Fe]                       | 4.22            | 4.21             | 4.23              | 4.22               | 4.23              | 4.24             | 4.29              | 4.33               | 2.88 |
| [La/Y]                        | 0.50            | 0.37             | 0.44              | 0.56               | 0.71              | 0.79             | 0.74              | 0.52               | 0.45 |
| [Pb/La]                       | 2.04            | 1.61             | 1.58              | 1.47               | 1.43              | 1.48             | 1.81              | 2.06               | 1.30 |

#### Acknowledgements

We are grateful to Roberto Gallino for helpful comments and discussions.

#### References

- Bisterzo, S., et al. 2010, MNRAS, in press, astro-ph:1001.5376v2  
 Campbell, S. W., Lattanzio, J. C. 2008, A&A, 490, 769  
 Cristallo, S., et al. 2009, ApJ, 696, 797 [C09]  
 Denissenkov, P. A., Tout, C. A. 2003, MNRAS, 340, 722  
 Gallino, R., et al. 1998, ApJ, 497, 388  
 Goriely, S., Mowlavi, N. 2000, A&A, 362, 599  
 Herwig, F., et al. 1997, A&A, 324, L81  
 Herwig, F., et al. 2003, ApJ, 593, 1056  
 Karakas, A., Lattanzio, J. 2003, PASA, 20, 279  
 Karakas, A., Lattanzio, J. 2007, PASA, 24, 103  
 Iben, I. Jr., Renzini, A., 1982, ApJ, 259, L79  
 Langer, N., et al., 1999, A&A, 346, L37  
 Siess, L., et al. 2004, A&A, 415, 1089  
 Straniero, O., et al. 1995, ApJ, 440, 85  
 Straniero, O., et al. 2003, PASA, 20, 389.  
 Straniero, O., et al. 2006, Nucl. Phys. A, 777, 311